Chinese Journal of Aeronautics, 2013,26(4): 898–908

Chinese Society of Aeronautics and Astronautics
& Beihang University

Chinese Journal of Aeronautics

cja@buaa.edu.cn
www.sciencedirect.com

Numerical investigation on jet interaction with a compression ramp

Zhen Huaping, Gao Zhenxun, Lee Chunhian *

School of Aeronautic Science and Engineering, Beihang University, Beijing 100191, China

Received 14 May 2012; revised 20 September 2012; accepted 13 December 2012
Available online 30 April 2013

KEYWORDS

Air pressure;
Amplification factor;
Computational aerodynamics;
Navier–Stokes equations;
Pitch control;
Transverse jet

Abstract A numerical investigation on jet interaction in supersonic laminar flow with a compression ramp is performed utilizing the AUSMDV scheme and a parallel solver. Several parameters dominating the interference flowfield are studied after defining the relative increment of normal force and the jet amplification factor as the evaluation criterion of jet control performance. The computational results show that most features of the interaction flowfield between the transverse jet and the ramp are similar to those between a jet and a flat plate, except that the flow structures are more complicated and the low-pressure region behind the jet is less extensive. The relative force increment and the jet amplification factor both increase with the distance between the jet and the ramp shortening till quintuple jet diameters. Inconspicuous difference is observed between the jet-before-ramp and jet-on-ramp cases. The variation of the injection angle changes the extent of the separation region, the plateau pressure, and the peak pressure near the jet. In the present computational conditions, 120° is indicated relatively optimal among all the injection angles studied. For cold gas simulations, although little influence of the jet temperature on the pressure distribution near the jet is observed under the computation model and the flow parameters studied, reducing jet temperature somehow benefits the improvement of the normal force and the jet efficiency. When the pressure ratio of jet to freestream is fixed, the relative force increment varies little when increasing the freestream Mach number, while the jet amplification factor increases.

1. Introduction

Aerodynamic control surfaces and transverse jets are two major strategies of attitude control for modern high-speed vehicles.[1] For instance, the advanced hypersonic glider vehicle HTV-2 takes use of both body flaps and reaction control system (RCS). Well-designed control surfaces are employed widely on airplanes and tactical missiles due to their high efficiency at low and modest altitudes. However, conventional control surfaces are ineffective for an extremely fast-moving vehicle maneuvering at high altitudes where dynamic pressures are rather low. Instead, transverse jets are ideal for enhancing the control performance of such an advanced concept because of their rapid response time as well as their ability to perform over a wide range of speeds and altitudes.[2,3] Furthermore, a combination of both aerodynamic surfaces and transverse jets satisfies all the control needs at various conditions,[4] making it the most potential scheme for future vehicle control.

* Corresponding author. Tel.: +86 10 82317011.
E-mail addresses: tracypp16@163.com (H. Zhen), gaozhenxun@163.com (Z. Gao), lichx@buaa.edu.cn (C. Lee).

Peer review under responsibility of Editorial Committee of CJA.

1000-9361
http://dx.doi.org/10.1016/j.cja.2013.04.026

The study of transverse jet control has received significant amount of interests for years owing to its complicated flow features, which consist of shock waves, boundary layer separations, shear layers, vortical structures, and complex interactions between them.[5–7] The surface pressure induced by the interference flowfield leads to an alteration in effective jet thrust force and, consequently, in control performance. Although a great deal of research has been performed,[8] there remain problems unresolved both in the context of flow mechanisms and engineering applications.

The flow feature of a jet injected into a cross flow is controlled by numerous parameters, such as the location of the jet, the flow conditions imposed on the jet and the freestream, and the geometric characteristics. Letko[9] investigated experimentally the effects of sonic and supersonic jets injected normally into a turbulent boundary layer over a flat plate under different pressure ratios. The freestream Mach number was set to be 4.5. Following the surface pressure mappings on the flat plate and the computed thrust augmentation, he claimed that a supersonic nozzle was more effective than a sonic nozzle as a control thruster, and an amount of 12% increase in effectiveness, after cutting the zone of negative pressure coefficient C_p behind the injector, could be attained. The experimental work conducted by Zukoski and Spaid[10] employed nitrogen, helium, and argon as working media injected normally with sonic speed into the boundary layer over a flat plate. The tests were run under different freestream Mach numbers, states of the boundary layer, pressure ratios, as well as injector diameters. An analytical model was developed by correlating those flow parameters with a dimensionless scaling parameter characterizing the forces acting on the flat plate. The model was partially successful, since the proposed correlation could work well only for a very restricted number of cases in certain regions and in turbulent boundary layers.

Clark and Chan[11] used the two-dimensional data provided by Aso et al.[12] to validate their numerical code, and then performed a parametric study on the influences of the injection angle to the wall pressure distribution and the normal force. Their results showed that, canting the injector 60° forward, i.e., against the freestream, would produce a normal force of 15% greater than that produced by a normal injector with the same jet mass flow rate. Byun et al.[13] attempted to utilize a three-dimensional ramp located downstream from an injector to alleviate the undesirable nose-down pitching moment typical in a jet interaction problem. The tests were conducted at a freestream Mach number of 4 with a sonic jet at a stagnation pressure ratio of 532. They finally concluded that the pitching moment coefficient of the jet-plus-ramp case was reduced by almost 70% with respect to the jet-only case without a net force loss. The advantage of this configuration exposes a promising technique for improving flight control performances. Nevertheless, a comprehensive investigation involving the effects of jet locations and flow parameters remains to be done so as to optimize the design and obtain the maximum control efficiency.

Most experimental studies are for turbulent jet interaction problems and corresponding computational simulations employ various turbulence models from algebraic models to the Reynolds stress models. Inadequate turbulence modeling has often been held responsible for disagreement between experiments and computations. While in theory higher-order turbulence modeling should perform better than lower-order one, some research has reported inconsistent results. For example, Clark and Chan[14] observed no improvement in using the k-ε model as compared with the Baldwin–Lomax algebraic model but significant changes of results against streamwise grid resolution. Viti et al.[15] tested the Spalart–Allmaras model, the Wilcox k-ω model, and the Reynolds stress model in the Mach 4 flowfield created by a ramp with sonic transverse injection. They found that the Reynolds stress computations were unable to obtain a converged solution, while the other two models presented differences in the separation region ahead of the injector. Considering the controversial aspects in turbulence modeling for this complicated flow problem, it is desirable to investigate the numerical accuracy of computational simulation of jet interaction to exclude the influence of numerical dissipation on the judgment of different turbulence models.

The purpose of this paper is to investigate the interaction phenomenon between a transverse jet and the supersonic flowfield around a control surface, in order to provide a preliminary understanding of an integrated attitude control technique based on the coupled reaction control and aerodynamic surface control concept. Laminar calculations are chosen to prove the capability of the numerical approach to accurately describe the jet interaction flowfield without any added computational burden and added complication of a turbulence model. In spite of the low possibility of encountering a laminar boundary layer in practical applications of jet thrusters, laminar conditions are reasonable when a vehicle is flying at high altitudes where the atmospheric density is low enough to reduce the Reynolds number below transition. The problem of a deflected aero-control surface is simplified and simulated as a three-dimensional flow over a compression ramp formed by the intersection of a flat plate and a wedge in the present study. The transverse jet can be located either upstream from the ramp or on the ramp. A numerical code based on the AUSMDV scheme with a parallel computing capability is developed and validated using a jet/flat-plate interaction case, whose experimental data readily exist. Based on the criterion for evaluating jet control effectiveness, the prominent features of the jet/ramp interaction flowfield are then studied systematically, and parameters governing the features are identified.

2. Numerical method

Laminar calculations are chosen in the present simulation for the reasons aforementioned. The Navier–Stokes equations neglecting body forces can be written in a conservational form as follows:

$$\begin{cases} \dfrac{\partial \rho}{\partial t} + \dfrac{\partial}{\partial x_j}(\rho u_j) = 0 \\ \dfrac{\partial (\rho u_i)}{\partial t} + \dfrac{\partial}{\partial x_j}(\rho u_i u_j + \delta_{ij} p) = \dfrac{\partial \tau_{ij}}{\partial x_j} \\ \dfrac{\partial (\rho E)}{\partial t} + \dfrac{\partial}{\partial x_j}(\rho H u_j) = \dfrac{\partial}{\partial x_j}\left(\tau_{ij} u_i + k \dfrac{\partial T}{\partial x_j}\right) \end{cases} \tag{1}$$

where ρ, p and T denote flow density, pressure, and temperature, respectively; u_j is the velocity component along the Cartesian coordinate x_j; E and H are the total energy and the total enthalpy per unit volume, respectively; τ_{ij} is the molecular viscous stress tensor; k is the heat transfer coefficient, and δ_{ij} is the Kronecker delta. The equation of state of perfect gas is introduced to close the system.

The convective flux vectors in Eq. (1) are computed using the AUSMDV scheme in conjunction with the MUSCL procedure to achieve second-order accuracy. The viscous terms are discretized using the standard second-order central difference scheme. The implicit LU-SGS (Lower–Upper Symmetric Gauss–Seidel) method is employed for time integration. The boundary conditions are set as follows: all the dependent variables are assigned their respective freestream values on the entry plane, and are extrapolated from interior flowfield on the top, the side, and the exit planes; non-slip and adiabatic wall conditions for the velocity and temperature fields, respectively, are applied to the solid surface; the parameters of jet exit, namely, the Mach number, the injection angle, the static temperature, and the jet-to-freestream pressure ratio are directly imposed at the cells simulating the circular injector. A parallel computing code is constructed to accomplish the simulation on multi-block grids. At the interface of each block, data is transferred using an message passing interface (MPI) protocol. The details of the numerical method with its additional applications are available in Ref. [16].

3. Code validation

3.1. Case description

The numerical code developed is validated through the classic experiment of a sonic circular jet on a flat plate in supersonic flows performed by Cubbison et al.[17] The numerical results computed by the present code are also compared with those computed by Viti.[18] A schematic layout of the experimental setup is shown in Fig. 1, together with the characteristic dimensions of both the flat plate and the injector. The distance from the leading edge to the center of the injector, L_0, was taken as a reference length for characterizing the dimensionless scales of the interacting flowfield. In the present case, the ratio of the reference length to the injector diameter d was fixed to be $L_0/d = 40$. Air was used as the working gas in the experiment and the boundary layer state was reported to be laminar. Flow conditions for both the freestream and the jet are listed in Table 1.

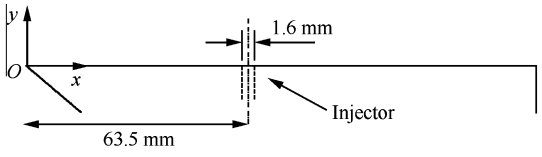

Fig. 1 Schematic layout of experimental setup.

Table 1 Flow conditions for Cubbison's test case.

Flow conditions	*Ma*	*p* (kPa)	*T* (K)
Freestream	2.92	1.05	107.6
Normal jet	1.0	357.4	280

Since the flowfield is symmetric about the xOy plane, only half the model is simulated in the present case. A structural grid system composed of seven blocks and 278833 points in total is utilized in the computations. Fig. 2 displays the global grid topology and the details of grid points clustering near the injector and the wall.

3.2. Computational results

The Mach number contours on the plane of symmetry depicted in Fig. 3 reveal globally the prominent features in the flowfield of the jet/plate interaction. When a jet is injected through a circular sonic nozzle into the supersonic freestream at a much higher static pressure, the gas immediately forms a Prandtl–Meyer expansion fan and is bended downstream by the incoming cross flow. The over-expanded gas is recompressed through a barrel shock wave and a Mach disk, and trails in the jet plume far downstream from the injection location. The barrel shock acts as a blunt obstacle to the freestream. A region of separated flow is created by the pressure rise as the cross flow stagnates ahead of the jet, where it induces a separation shock. An extensive low-pressure, separated region also forms in the jet wake, as shown in Fig. 4. The separation and reattachment lines are the tracks showing the existences of the horse-shoe vortex and secondary separation vortex in the recirculation zone upstream from the jet.

Fig. 5 presents the comparison of pressure coefficient distributions on the flat plate surface given by a previous experiment[17] (upper half) and the present computation (bottom half), which shows an overall good agreement. The distribution of C_p along the centerline is compared in Fig. 6 with the experiment data as well as the numerical results given by Viti.[18]

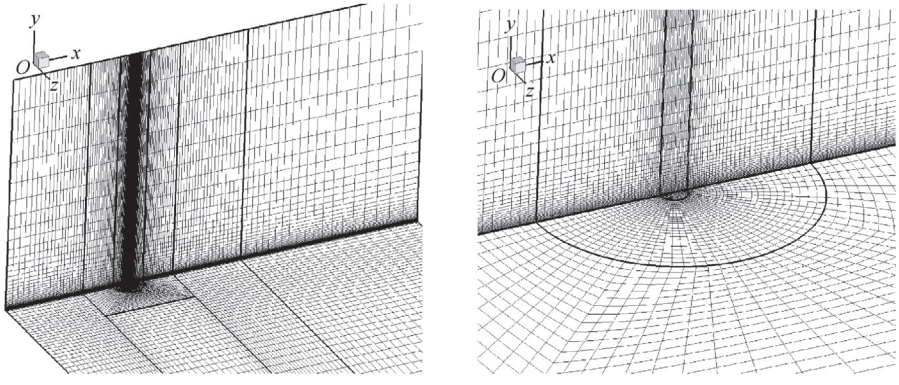

(a) Near the injector (b) Near the wall

Fig. 2 Global grid and details around the injector.

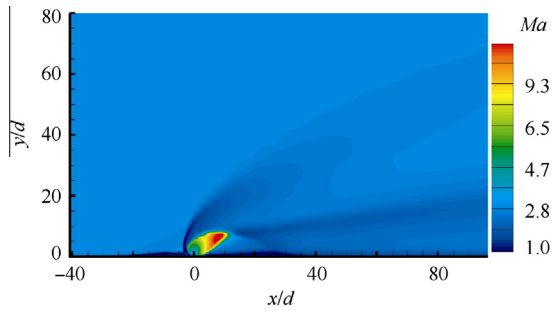

Fig. 3 Mach number contours on the symmetric plane for validation case.

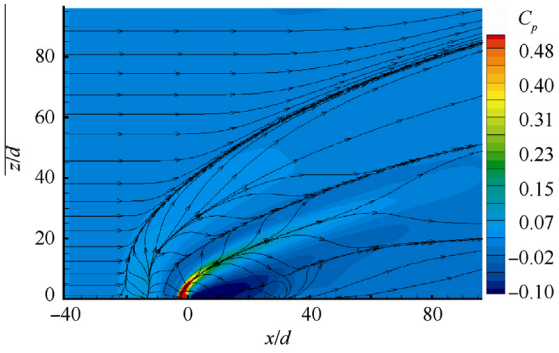

Fig. 4 Separation and reattachment lines superimposed on pressure contours of the plate surface.

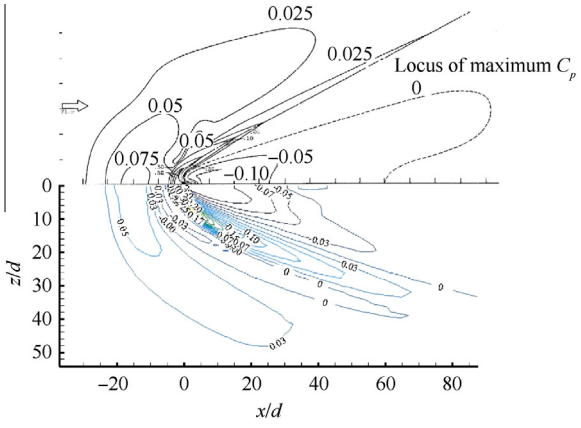

Fig. 5 Comparison of pressure coefficient contour lines on the flat plate surface for validation case.

It is noticeable that the present results agree well with Viti's computational results, whereas both underpredict the pressure close to the jet. The discrepancy is probably caused by computation model, grid quality, or experimental uncertainty. Viti attributed it to the unsatisfactory grid cells used in the separation region, and introduced a more complex grid topology.[18] Due to the complexity of jet interaction flowfield, more grid cells are needed in the separation region to obtain a precise simulation. Considering that the total number of grid points in the validation computation is just 1/3 of that adopted by

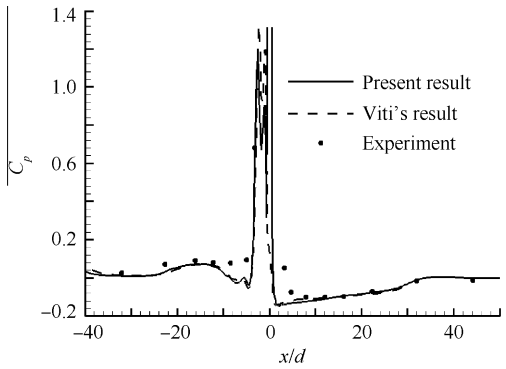

Fig. 6 Comparison of pressure coefficient distributions along the centerline for validation case.

Viti,[18] the present code appears more capable of capturing jet interaction flow structures.

In summary, the above comparisons and analysis demonstrate that the developed numerical method can well capture both shock structures and wall pressure distributions of a jet interaction flowfield. This ensures that reliable conclusions can be drawn in the following research on jet control performance.

4. Evaluation criterion

The jet amplification factor K has been widely adopted to evaluate the force augmentation of the interaction between the transverse jet and the cross flow. However, its definition was not unified in different work. Spaid and Cassel[19] defined the amplification factor as $K_F = (F_i + T_j)/T_{jSV}$, where F_i and T_j are the interaction force and the jet thrust, respectively, and T_{jSV} is the vacuum thrust of a sonic jet having the same stagnation conditions and mass flow rate as an actual jet. Mostly, T_j was used directly as the denominator to give another expression as $K_F = (T_j + \Delta T_j)/T_j = (F_{jeton} - F_{jetoff})/T_j$,[20] where F_{jeton} and F_{jetoff} represented the aerodynamic force with and without the jet, respectively, and ΔT_j is the induced force, respectively. The same value could be obtained using aerodynamic coefficients instead. However, Cheng et al.[21,22] named it the jet efficiency, and defined their own augmentation factor as $K_{Cn} = C_{nwj}/(C_{nw0} + C_{n0j})$, where the subscripts wj, w0, and 0j denote the cases of wind-plus-jet, wind-only, and jet-only, respectively.

In practical applications, the amount of the induced force added to the initial case, as well as the ratio of the induced force to direct jet thrust, are two key design parameters. To make the procedure convenient, the former is called the relative force increment denoted by V, and the latter the jet amplification factor denoted by K in this study. The two parameters together can evaluate comprehensively the performances of the jet/cross flow interaction. Their expressions are written in dimensionless forms as follows:

$$V = \frac{C_{nwj} - C_{nw0}}{C_{nw0}} \tag{2}$$

$$K = \frac{C_{nwj} - C_{nw0}}{T_j/(q_\infty S)} \tag{3}$$

where C_{nwj} and C_{nw0} are the normal force coefficients for the cases of wind-plus-jet and wind-only, respectively; q_∞ and S

the dynamic pressure and the reference area, respectively. T_j is calculated using jet exit conditions as follows:

$$T_j = m_j v_j + (p_j - p_\infty) A_j \quad (4)$$

where m_j, v_j, and A_j are the jet mass flow rate, jet exit velocity, and jet exit area, respectively; p_j and p_∞ are the jet exit pressure and freestream pressure, respectively.

For different geometric configurations, V and K change with the jet strength, which can usually be predicted by pressure ratio, mass flow ratio, momentum ratio, etc. In this work, the pressure ratio PR = p_j/p_∞ is preferred, since the gas specific heat ratio, the jet exit Mach number, and the nozzle diameter all remain constant.

5. Jet interaction with a ramp

The flowfield over a ramp formed by an intersection of a flat plate with a wedge, usually referred as a compression corner, is a simplified model representing the flow around a deflected aerodynamic control surface. When a transverse jet is introduced, the interaction between them causes the initial pressure distributions change, leading to a variation of overall forces loaded on the surface. A parametric study is performed on this model by varying the location of the jet, the injection angle, the jet temperature, and the freestream Mach number.

5.1. Comparison between jet/ramp and jet/plate cases

The configuration is sketched in Fig. 7 together with characteristic dimensions denoted. The injector has a diameter of d = 1 mm. The distance from the jet exit to the hinge line of the ramp is $L = 5d$. The ramp with a length of $L_r = 20d$ is deflected at an angel of $\beta = 10°$. The atmospheric conditions at an altitude of 35 km are chosen for the incoming flow. The pressure ratio of the normal jet to the freestream is PR = 50. The flow conditions of both the freestream and the jet are listed in Table 2. A half model in z direction is also chosen in the present simulation due to the flowfield being symmetric about the xOy plane. The grid generation follows the same approach as that in Section 3.1. The model of the jet/plate interaction case is easily obtained when $\beta = 0°$, while other flow parameters remain the same.

Mach number contours on the symmetric planes of both cases are compared in Fig. 8(a) and (b). Both cases show similar flow features characterized by barrel shock, Mach disk, lambda shock, and separation region. However, the shape of the shock structure for the jet/ramp case differs from that for the jet/plate case, demonstrating that a more complicated interaction occurs between the ramp and the shock. The characteristics can also be observed from C_p distributions in Fig. 9, where along the centerline, the magnitude of the high pressure upstream from the jet for the jet/ramp case shows slightly greater than that for the jet/plate case, while the low pressure downstream from the jet becomes substantially higher. Fig. 10 helps in understanding the pressure distributions over the whole surface. The high-pressure region moves more upstream from the jet in the jet/ramp case (upper half), meanwhile the extent of the low-pressure region downstream from the jet in the jet/ramp case is much smaller than that in the jet/plate case (lower half).

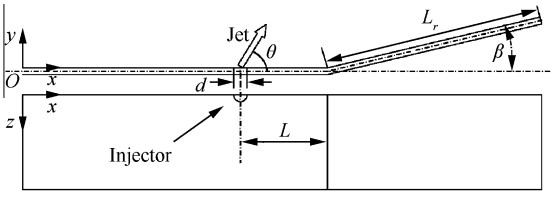

Fig. 7 Configuration for a jet/ramp interaction case.

Table 2 Flow conditions for jet/ramp interaction.

Flow conditions	*Ma*	*p* (kPa)	*T* (K)
Freestream	4.0	0.575	236.5
Jet	1.0	28.75	236.5

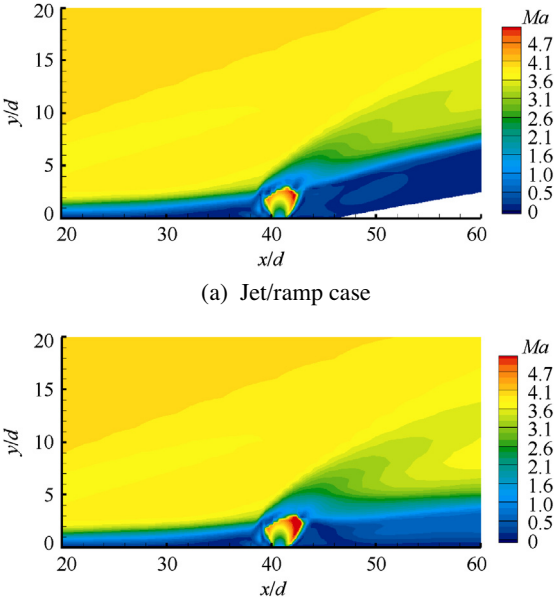

(a) Jet/ramp case

(b) Jet/plate case

Fig. 8 Comparison of Mach number contours on the symmetric plane between jet/ramp and jet/plate cases.

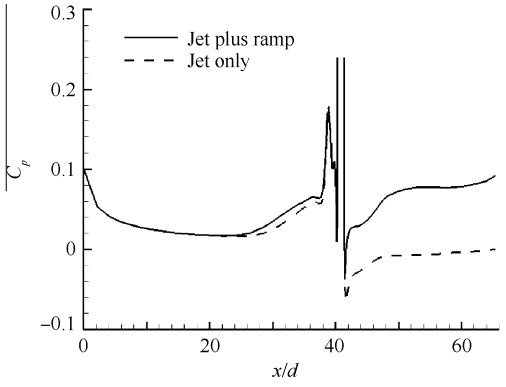

Fig. 9 Comparison of pressure coefficient along the centerline between jet/ramp and jet/plate cases.

5.2. Influences of jet location

5.2.1. Problem description

The configuration for the present test case follows the model shown in Fig. 7. All parameters are chosen to be the same as those considered in the previous test case, except for L. Here, the computations are performed for different L, i.e., the circular jet is placed at the location of $L = 2d$, $5d$, and $10d$ before the ramp, respectively, and additionally at $L = 5d$ on the ramp. Parametric study is also performed for different pressure ratios to observe the variations of the relative force increment and the jet amplification factor with respect to different assigned conditions.

5.2.2. Results and analysis

Mach number contours on the planes of symmetry and pressure coefficient contours on the solid surface for different locations of the jet at a pressure ratio of 100 are compared in Figs. 11 and 12, respectively. As seen in the plots, the bulk characteristics of the interaction flowfield, such as Mach disk, bow shock, and separation shock remain the same as in the previous cases. For the cases of jet-before-ramp, the separated region extends more upstream as L increases, while the low-pressure region aft of the jet extends more downstream. Comparing Fig. 11(b) with Fig. 11(d), and Fig. 12(b) with Fig. 12(d), it is evident that the onset locations of the separated region in the x direction are almost the same for the cases of jet-before-ramp and jet-on-ramp, despite their shock strengths and separation lengths are different.

The variation of relative force increments, with given pressure ratios at different locations before the ramp, is depicted in Fig. 13. In all cases, V increases nonlinearly with increasing PR, but more rapidly with lower pressure ratios than with the higher ones. In addition, the distribution of V for $L = 10d$ lies beneath those of the remaining two cases which are close to each other. The decreasing of the jet amplification factor illustrated in Fig. 14 possesses a similar trend, i.e., the whole level of K for $L = 10d$ falls under those of the remaining cases, whose differences are negligible.

Figs. 15 and 16 compare, respectively, the relative force increment and the jet amplification factor of the jet-on-ramp case with those of the jet-before-ramp case. Their variations with respect to the pressure ratios share a similar trend. For the former case, both parameters are smaller when pressure ratio is less than 100, whereafter they exceed their latter counterparts. However, the differences between these two cases are not significant enough to distinguish them apart.

In summary, both the relative force increment and the jet amplification factor increase as the distance between the jet exit and the hinge line of the ramp is shortened till five times of the injector diameter, and then keep nearly unchanged.

Within parametric ranges considered in the present parametric study, minor differences are observed between the cases of jet-on-ramp and jet-before-ramp. As a consequence, it is

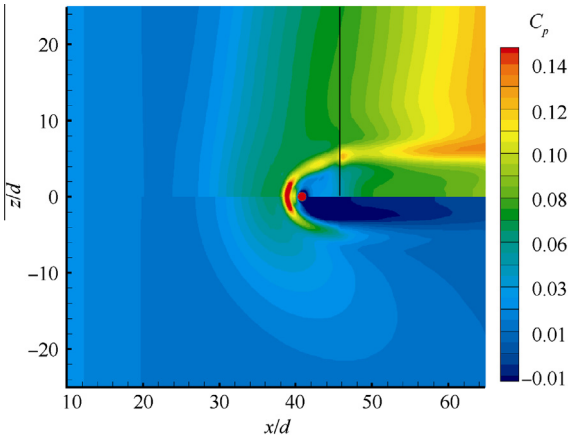

Fig. 10 Comparison of pressure coefficient contours on the wall between jet/ramp and jet/plate cases.

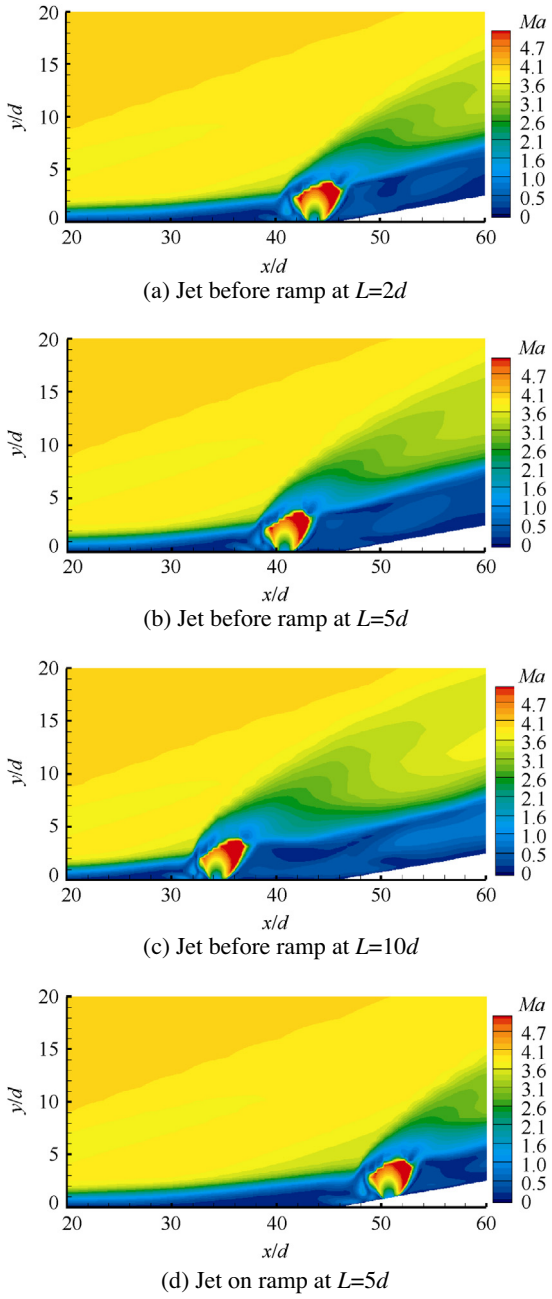

Fig. 11 Mach number contours on the symmetric planes at PR = 100.

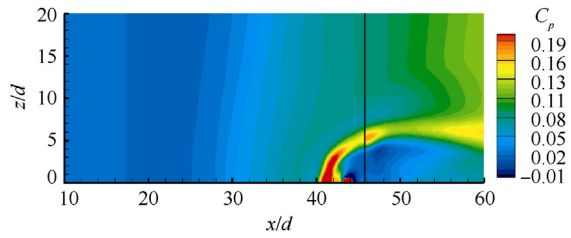

(a) Jet before ramp at L=2d

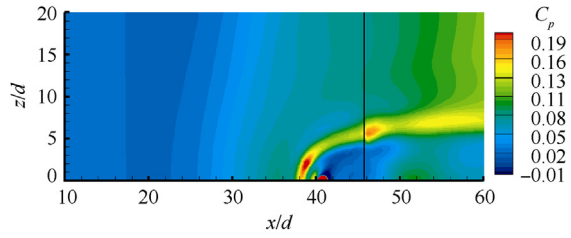

(b) Jet before ramp at L=5d

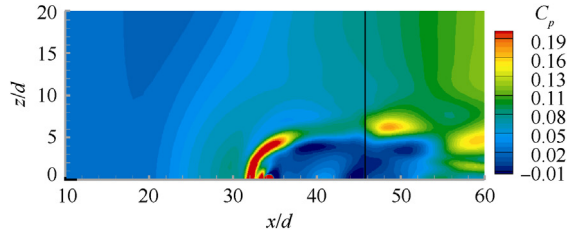

(c) Jet before ramp at L=10d

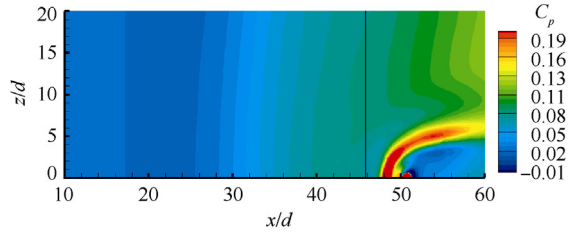

(d) Jet on ramp at L=5d

Fig. 12 Pressure coefficient contours on the walls at PR = 100.

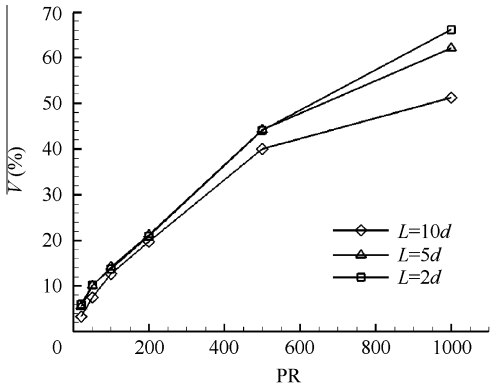

Fig. 13 Variations of relative force increments with given pressure ratios for different jet locations before the ramp.

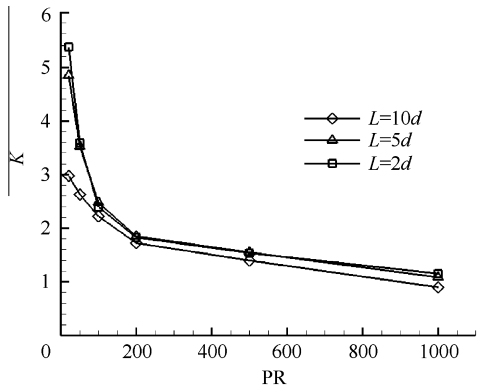

Fig. 14 Variations of jet amplification factor with given pressure ratios for different jet locations before the ramp.

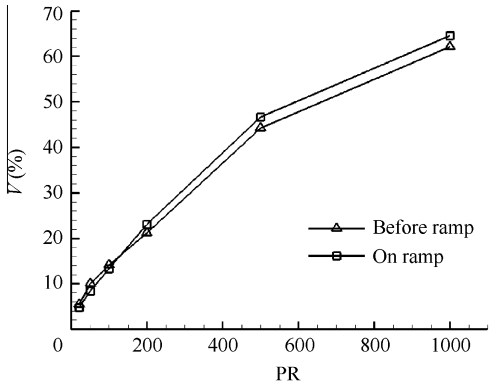

Fig. 15 Comparison of relative force increments between jet-before-ramp and jet-on-ramp cases.

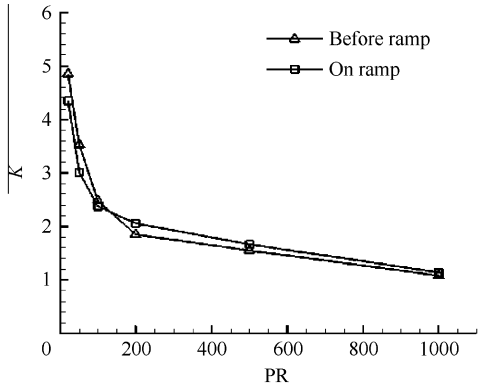

Fig. 16 Comparison of jet amplification factor between jet-before-ramp and jet-on-ramp cases.

preferred in the following computations to utilize the model with the jet located at L = 5d before the ramp.

5.3. Influences of jet injection angle

5.3.1. Problem description

The influences of the jet injection angle are studied on the jet-before-ramp configuration, as aforementioned, with all

geometric and flow conditions remaining the same as in Section 5.1. The injection angle is defined as the angle of the axis of the jet exit inclining from the direction of the freestream, depicted in Fig. 7. It is precisely, in the current coordinate system, the supplementary angle of that defined in Ref. [11]. Five injection angles, i.e., 60°, 90°, 105°, 120°, and 135°, together with different pressure ratios are computed.

In Eq. (3), the denominator representing the jet thrust is calculated for the injection normal to the exit cross section. Under the same exit Mach number and pressure ratio, the change of the injection angle leads to an alteration on vectoring thrust. Hence, it is more reasonable to take the jet thrust in the injection angle of 90° as the baseline for predicting the jet amplification factor. The values of K in this section are determined under such considerations.

5.3.2. Results and analysis

Fig. 17 depicts the pressure coefficient distributions along the centerlines for the five injection angles at a pressure ratio of 100. The separation region ahead of the jet extends progressively upstream, and the peak of the pressure distribution also rises with the injection angle ranging from 60° to 120°. Then, the peak of the pressure distribution declines, e.g., the value for the injection angle of 135° drops even lower than the one for the injection angle of 105°. The tendency on achieving a maximum interaction mechanism in the vicinity of 120° seems in consistent with the existing observations on jet/plate interaction cases given in Refs. [11,23].

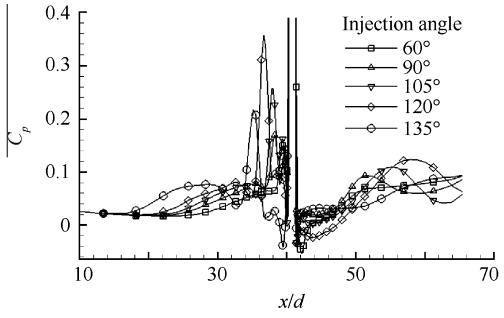

Fig. 17 Comparison of pressure coefficient along the centerlines for different injection angles at PR = 100.

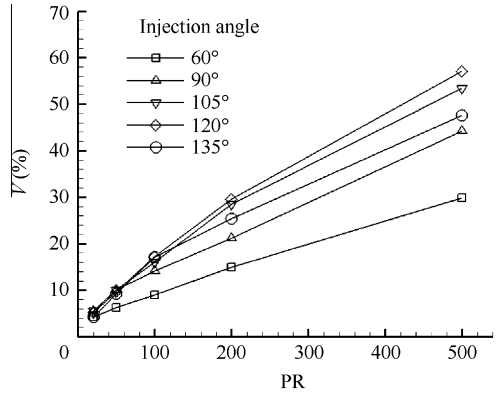

Fig. 18 Comparison of relative force increment with pressure ratios for different injection angles.

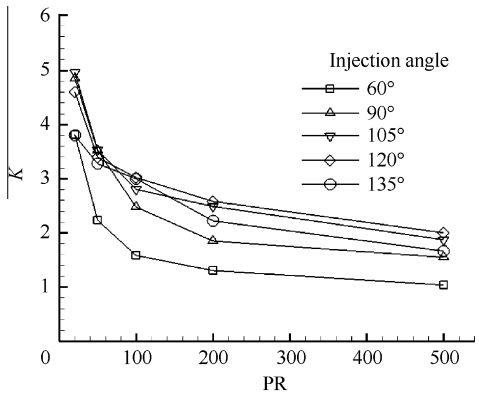

Fig. 19 Comparison of jet amplification factor with pressure ratios for different injection angles.

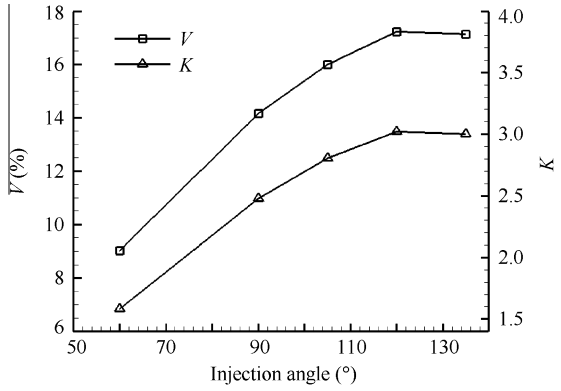

Fig. 20 Variations of relative force increment and jet amplification factor with injection angles at PR = 100.

Figs. 18 and 19 compare the variations of the relative force increment and the jet amplification factor under various pressure ratios, respectively. The relative force increments increase while the jet amplification factors decrease with increasing PR for all the five injection angles. At a fixed pressure ratio, both parameters increase gradually with the injection angle varying from 60° to 120°, and then decrease. The trend can be more clearly seen in Fig. 20, which gives the variations of the relative force increment and the jet amplification factor with jet injection angles at a pressure ratio of 100.

The analysis presented above indicates that 120° is the optimal injection angle to accomplish the most effective jet/ramp interactions. This injection angle can thus be selected as the thrust vectoring angle for controlling the aerodynamic forces of compression ramps within the parametric ranges specified in the present parametric study.

5.4. Influences of jet temperature

5.4.1. Problem description

There are two types of commonly employed reaction control systems, namely, one with hot gas created by the combustion of propellant as the working medium, and the other with compressed cold gas. The present study focuses on the latter, without considering high-temperature effects or multi-species flows. The computational model and flow parameters chosen

in the present test case are still the same as those chosen in Section 5.1, except for the jet exit temperature ranging from 80 K to 300 K.

5.4.2. Results and analysis

Fig. 21 exhibits the pressure coefficients along the centerlines for different jet temperatures. No obvious differences in the distributions ahead of the jet are observed by increasing the jet exit temperature. Although C_p behind the jet changes notably, no inherent patterns are observed. As the jet pressure ratio being raised, the relative force increment shown in Fig. 22 increases, while the jet amplification factor shown in Fig. 23 decreases. The results show a similar trend to those given in Sections 5.1 and 5.2. This is easy to understand for the variation in the jet temperature in cold gas simulations is just the variation in the mass flow rate which in essential is the reason for results of the pressure variation.

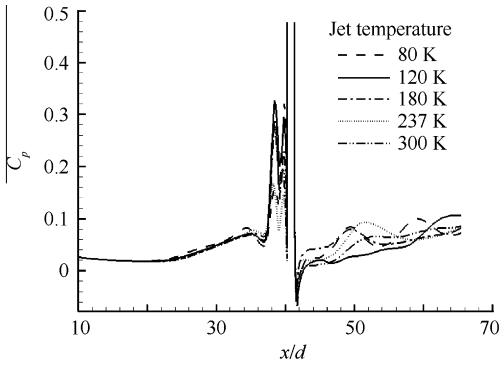

Fig. 21 Comparison of pressure coefficient along the centerlines for different jet temperatures at PR = 100.

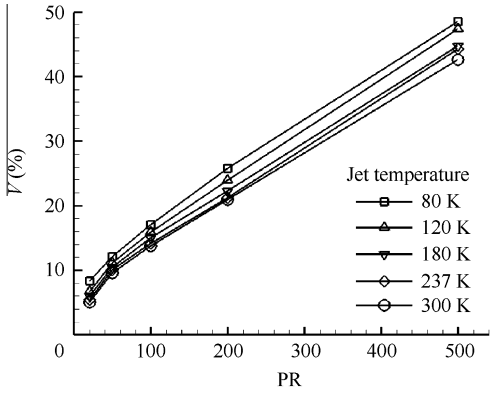

Fig. 22 Comparison of relative force increment with pressure ratios for different jet temperatures.

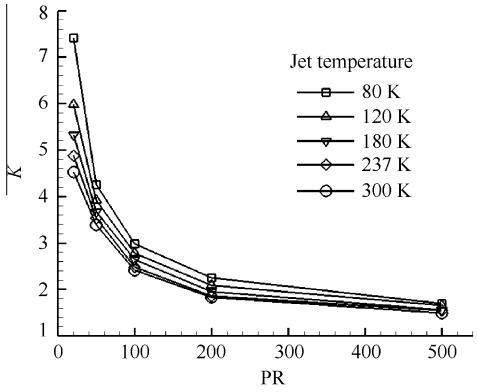

Fig. 23 Comparison of jet amplification factor with pressure ratios for different jet temperatures.

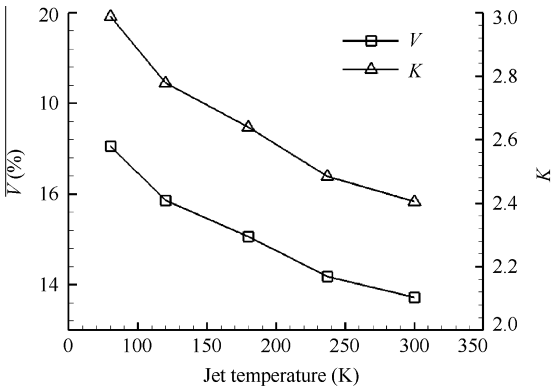

Fig. 24 Variations of relative force increment and jet amplification factor with jet temperatures at PR = 100.

As shown in Fig. 24, both parameters decrease with increasing jet temperature when the jet pressure ratio is fixed at PR = 100, indicating that low jet temperature may benefit the improvement of the jet control effectiveness. However, the temperature must not be too low to let a phase change take place in the jet gas, which may lead to alterations of flow characteristics. Apparently, further study on the influences of the jet temperature on the reaction control efficiency is needed.

5.5. Influences of freestream Mach number

5.5.1. Problem description

Influences of the freestream Mach number on the interaction flowfield are discussed in this section. The jet-before-ramp model shown in Fig. 7 is considered, together with the flow parameters specified in Section 5.1. A parametric study is conducted for Mach numbers ranging from 2 to 6.

Since the freestream Mach number Ma_∞ is contained in the expression of the surface pressure coefficient C_p, in order to investigate the influences of the Mach number to the interaction flowfield, another dimensionless parameter p/p_1 is utilized to replace C_p for representing the pressure distribution in this section. Here, p_1 is the wall pressure of a flat plate sharing the same geometric characteristics as the ramp model for a specified Ma_∞.

5.5.2. Results and analysis

Fig. 25 shows the centerline pressure distributions for Ma_∞ = 2, 3, 4, 5, and 6 at PR = 50. All the upstream pressure distributions exhibit similar patterns, consisting of a pressure plateau, a peak pressure followed by an expansion fan, then a small pressure rise, and finally a thin region of over-expansion. There are two significant flow developments observed in the parametric computations. As Ma_∞ increases, the peak pressure increases and moves downstream. Additionally, the

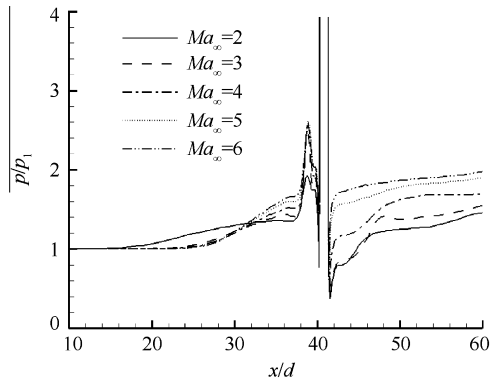

Fig. 25 Comparison of C_p along the centerlines for different freestream Mach numbers at PR = 50.

initial pressure rise leading to the pressure plateau moves downstream as Ma_∞ increases, but settles to a constant location for Ma_∞ greater than 3.0. The characteristic is analogous to the hypersonic limit seen in detached shocks on blunted bodies.[24] The downstream pressure distributions exhibit similar characteristics as well. An initial large over-expansion is followed by a pressure rise, where in some cases a pseudo-plateau forms, and finally it overshoots the ambient pressure. As Ma_∞ increases, the location of the overshoot moves upstream, representing the low-pressure region behind the jet diminishes in some extent.

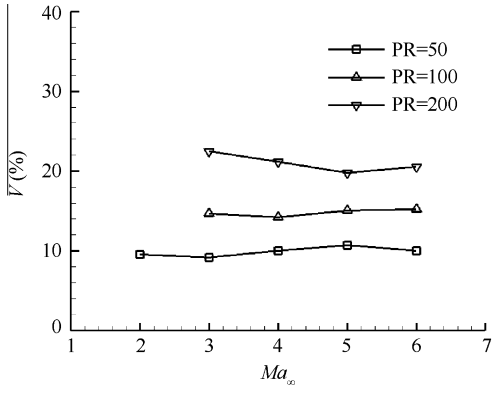

Fig. 26 Variation of relative force increment with freestream Mach number.

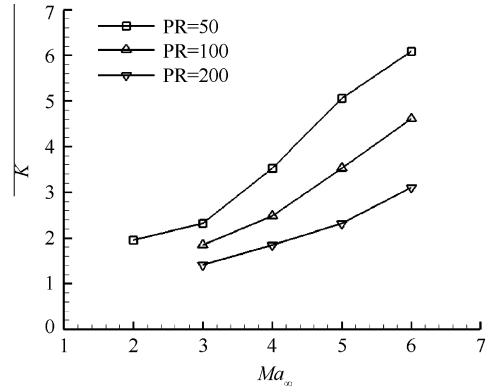

Fig. 27 Variation of jet amplification factor with freestream Mach number.

Figs. 26 and 27 depict the relative force increment and the jet amplification factor with freestream Mach number, respectively. Within the range of Ma_∞ under consideration, no prominent difference is observed for V at a specified pressure ratio, which indicates that the interaction force is dominated mostly by the pressure ratio and insensitive to the freestream Mach number when other conditions are fixed. At each pressure ratio, the jet amplification factor increases with increasing Ma_∞, whose values are lower for higher pressure ratios and higher for lower ones. The trend is in consistent with the analysis made above. Incidentally, the separated region extends beyond the leading edge of the plate when the pressure ratio exceeds 100 at $Ma_\infty = 2$, wherefore the values of V and K are only available when PR = 50.

6. Conclusion

(1) The bulk characteristics of the interaction flowfield between jets and high Mach number flows over a ramp are similar to those exhibited between jets and high Mach number flows over a flat plate. However, the jet/ramp interacting flowfield may consist of slightly different shock configurations, more complicated flow structures, higher pressure levels ahead of the jet, and less extensive low-pressure regions behind the jet.

(2) The relative normal force increment and the jet amplification factor both increase as the distance between the jet and the ramp is shortened till quintuple jet diameters. The inception locations of the separated region in the x direction are found to be practically the same for both jet-before-ramp and jet-on-ramp cases. The differences in the relative force increment and the amplification factor between the two cases can be ignored.

(3) The variation of the injection angle changes the extents of the separation region, the pressure plateau, and the pressure peak in the vicinity of the jet. The angle of 120° is found to be relatively optimal within the range of injection angle in conditions studied in this paper.

(4) Little influences of the jet temperature onto the pressure distribution are observed under the adopted computation model and the ranges of flow parameters specified in the present parametric study. Nevertheless, reducing jet temperature may benefit the improvement of the combined control effectiveness.

(5) When the jet-to-freestream pressure ratio is fixed, the normal force is found insensitive to freestream Mach number with remaining conditions unchanged, while the jet amplification factor increases notably with increasing freestream Mach number.

Acknowledgement

The authors are grateful to the anonymous reviewers for their critical and constructive reviews of the manuscript.

References

1. Deng YG, Tian JT, Wang YF, Lei JW. Summarization of attitude control technology. *Control Technol Tactical Missile* 2006;**53**(2): 7–13 [Chinese].

2. Kang ZM. Research on hypersonic vehicle development strategy. *Modern Def Technol* 2000;**28**(4):27–33 [Chinese].
3. Li YL, Yang SX. Key technology analysis of blended control caused by lateral/aerodynamic forces for air defense missiles. *Acta Armamentarii* 2007;**28**(12):1523–7 [Chinese].
4. Wang WZ, He KF. Research on blended control caused by aerodynamic surface and RCS. In: Flight dynamics and flight test annual conference; Yichang, China; 2005.
5. Orth RC, Schetz JA, Billig FS. The interaction and penetration of gaseous jets in supersonic flow. NASA; 1969 Report No.: CR-1386.
6. Nakano MM, Williams RL. Space shuttle on orbit flight control, system. AIAA-99-0810; 1999.
7. Louis AC. Applying jet interaction technology. *J Spacecraft Rockets* 2003;**40**(4):523–37.
8. Margason RJ. Fifty years of jet in cross flow research. AGARD; 1993 Report No.: N94-28003.
9. Letko W. Loads induced on a flat plate at a Mach number of 4.5 with a sonic or supersonic jet exhausting normal to the surface. NASA; 1963 Report No.: TND-1935.
10. Zukoski EE, Spaid FW. Secondary injection of gases into a supersonic flow. *AIAA J* 1964;**2**(10):1689–96.
11. Clark SW, Chan SC. Numerical investigation of a transverse jet for supersonic aerodynamic, control. AIAA-92-0639; 1992.
12. Aso S, Okuyama S, Kawai M, Ando Y. Experimental study of mixing phenomena in supersonic flows with slot injection. AIAA-91-0016; 1991.
13. Byun YH, Bae KJ, Wallis S, Viti V, Schetz JA, Bowersox R. Jet interaction in supersonic flow with a downstream surface ramp. *J Spacecraft Rockets* 2005;**42**(1):38–44.
14. Clark SW, Chan SC. Effects of turbulence models and adaptive grids on the jet interaction flowfield. AIAA-93-3524; 1993.
15. Viti V, Schetz J, Neel R. Comparison of first and second order turbulence models for a jet/3D ramp combination in supersonic flow. AIAA-2005-1100; 2005.
16. Gao ZX. Study on modeling and numerical simulation for supersonic turbulence combustion flows [dissertation]. Beijing: School of Aeronautic Science and Engineering, Beihang University; 2011.
17. Cubbison RW, Anderson BH, Ward JJ. Surface pressure distribution with a sonic jet normal to adjacent flat surfaces at Mach 2.92 to 6.4. NASA; 1961 Report No.: TND-580.
18. Viti V. Numerical studies of the jet interaction flowfield with a main jet and an array of smaller jets [dissertation]. Blacksburg: Virginia Polytechnic Institute and State University; 2002.
19. Spaid FW, Cassel LA. Aerodynamic interference induced by reaction controls. AGARD; 1973 Report No.: AG-173.
20. Li SX. Physics of vehicle attitude control by jets. *Aerodyn Front Res* 2003;327–32.
21. Cheng KM, Wu YZ, Lv YW, et al. A study of gas dynamic gain performance of lateral jets. *Acta Aerodyn Sin* 2003;**21**(4):432–8 Chinese.
22. Gong JF, Cheng KM. On the interaction features of side-jet by the nozzle geometry. In: Second low transonic/supersonic aerodynamics Conference; 2002. p. 306–313.
23. Koch LN, Collins DJ. The effect of varying secondary Mach number and injection angle on secondary gaseous injection into a supersonic flow. AIAA-70-0552; 1970.
24. Dickmann DA, Lu FK. Jet in supersonic flow on a flat plate. AIAA-2006-3451; 2006.

Zhen Huaping received her B.S. degree in Engineering Mechanics from Beihang University in 2006, and then became a Ph.D. student there. Her main research interests are hypersonic aerodynamics, flow control, and hypersonic vehicle design.

Gao Zhenxun is a teacher in the School of Aeronautic Science and Engineering at Beihang University, where he received his B.S. and Ph. D degrees in 2005 and 2011, respectively. His area of research includes turbulent diffusion combustion, hypersonic vehicle design, and thermodynamics.

Lee Chunhian is a professor and Ph.D. advisor in the School of Aeronautic Science and Engineering at Beihang University. His current research interests are hypersonic aerodynamics, MHD generator, transition prediction, and hypersonic vehicle integrated design.